Level Crossing Rate Estimation (LCRE)

A New Technique for Finding GNSS Carrier to Noise Ratios

© iStockphoto.com/tamer yazici

The authors propose a new carrier-to-noise ratio (CNR) estimation method — an important metric in GNSS receiver operation — based on use of the level crossing rate of a receiver's correlation function.

ELENA-SIMONA LOHAN AND DANAI SKOURNETOU
TAMPERE UNIVERSITY OF TECHNOLOGY

Knowledge of carrier-to-noise ratio (CNR) can be of great value in the context of GNSS. In addition to determining the relative signal to noise strength, CNR information can assist various stages of signal tracking in a GNSS receiver. For example, CNR measurements may serve as status indicators of the code and carrier tracking loops by detecting the presence of loss-of-lock events. A receiver may also incorporate CNR estimates in its tracking stages for increasing the accuracy of the estimated synchronization parameters, enhancing multipath mitigation techniques, or as a triggering

mechanism for switching among tracking algorithms to optimize performance in various CNR ranges.

The multitude of possible applications for CNR measurements is far from being exhausted. In order to efficiently serve existing and future CNR-based applications, receiver designs that maximize estimation accuracy become paramount. Whilst the technical literature contains plenty of paradigms, many GNSS-specific estimation methods are limited by sensitivity to noise power or perform poorly performance in low CNR conditions.

Situations in which higher estimation accuracy is desired may lead to techniques that require higher computational complexity. Acknowledging this

trade-off, we propose a new CNR estimation technique called *level-crossing-rate estimation* (LCRE), which exhibits optimal performance under very noisy conditions.

Statistical Characterization of Signals

One of the main functions that a GNSS receiver performs is the cross-correlation of the received signal with a stored reference in order to match up the same pseudorandom noise (PRN) code. This process also incorporates a certain estimate of Doppler frequency and code delay.

Assuming the signal has been transmitted over an additive white Gaussian noise (AWGN) channel, we can model

the sampled output of the cross-correlation function as

$$x_R(nT_s) = x_R(n) =$$
$$= \sqrt{E_b}\, a_0 R_{mod}(\Delta\tau, \Delta_{f_D}) \exp\{-j2\pi\Delta_{f_D}n + \varphi_0\} + v(n) \quad \text{(1)}$$

where T_s is the sampling period; E_b stands for the data bit energy, and a_0 is the amplitude attenuation. Further, $R_{mod}(\Delta\tau, \Delta_{f_D})$ represents the auto-correlation function (ACF), defined here as the cross-correlation between the modulation waveform used in the receiver and the modulation waveform used for the reference signal, stored in the receiver. Moreover, $\Delta\tau$ and Δ_{f_D} are the code and frequency estimation errors, equal to $\hat{\tau} - \tau_0$ and $\hat{f}_D - f_D$, respectively; φ_0 is the carrier phase of the channel path, and $v(n)$ the complex noise term of the double-sided power spectral density $\frac{N_0}{2}$.

The shape of the ACF depends on the modulation scheme used on the transmitter side. However, if the receiver uses a different reference waveform, the correlation shape is also affected. For future GNSS signals, the composite binary offset carrier (CBOC) modulation scheme has been selected for mass-market applications. Here, we specifically use the CBOC ('-') implementation since it is the most probable candidate for future Galileo Open Service (OS) pilot signals.

CBOC consists of a superposition of two sine BOC waveforms: a sine BOC(1,1) and a sine BOC(6,1) component. Depending on whether we add or subtract the BOC components, we have a CBOC('+') or CBOC('-') implementation, respectively.

Although the majority of existing work on the subject assumes both the transmitted and reference signals to be CBOC modulated, recent studies show that processing the CBOC signal with a sine BOC(1,1) reduces the processing complexity and can be advantageous in cases of limited-bandwidth receivers. For this reason, in our study we assume the paired usage of a CBOC transmitter with a sine BOC receiver.

If we denote by x_I and x_Q the real and imaginary samples of x_R, after one millisecond of integration they clearly follow the statistics of the Gaussian noise term; therefore, both x_I and x_Q are Gaussian distributed with variance $\frac{N_0}{2}$. Moreover, we are able to categorize samples into two cases: (1) *peak point* (PP), for samples located within chip from the estimated code delay, because we assume the samples are situated on the main peak of the correlation function, and (2) *outside peak point* (OPP), for samples located outside two-chip interval.

Figure 1 illustrates examples of PPs and OPPs on the real part of the coherent cross-correlation function (CCF) in an additive white Gaussian noise (AWGN) channel.

In a straightforward way, we statistically characterize the real and imaginary samples based on whether they correspond to a PP (indicated with the subscript *p*) or an OPP (indicated with the subscript *o*) as

$$\begin{cases} x_{I,p} \sim N\left(\sqrt{\hat{E}_b}, \dfrac{N_0}{2}\right) \\ \\ x_{I,o}, x_{Q,p}, x_{Q,o} \sim N\left(0, \dfrac{N_0}{2}\right) \end{cases} \quad \text{(2)}$$
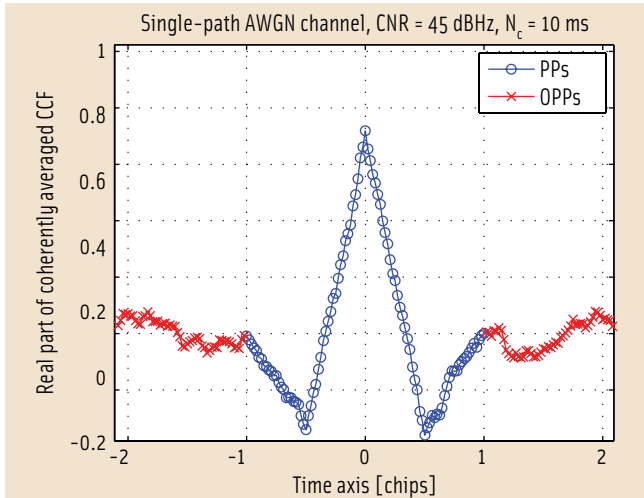
FIGURE 1 **Example of peak points (PPs) and outside peak points (OPPs) on the real part of the coherently-averaged CCF in AWGN channel.**

where $\hat{E}_b$ represents the equivalent bit energy, defined as $E_b a_0^2 R_{\text{mod}}^2 \left(\Delta\tau, \Delta_{f_D} \right)$.

Typically, a receiver applies both coherent and non-coherent averaging to the output of the CCF for better robustness against noise. If we denote the coherent integration time by N_c (in milliseconds), we can express the real and imaginary parts of the coherent correlation function as

$$\begin{cases} y_I = \dfrac{1}{N_c} \sum_{nc=1}^{N_c} x_{I,nc} \\ y_Q = \dfrac{1}{N_c} \sum_{nc=1}^{N_c} x_{I,nc} \end{cases}$$ (3)

While y_I and y_Q remain Gaussian distributed, their statistics are now defined as

$$\begin{cases} y_{I,p} \sim N\left(\sqrt{\hat{E}_b}, \dfrac{N_0}{2N_c} \right) \\ y_{I,o}, y_{Q,p}, y_{Q,o} \sim N\left(0, \dfrac{N_0}{2N_c} \right) \end{cases}$$ (4)

If for statistical simplicity we assume that the squared envelopes are used for the formation of the non-coherent decision variable, we can write the output as

$$z = \frac{1}{N_{nc}} \left(\sum_{nc}^{N_{nc}} y_{I,nnc}^2 + \sum_{nc}^{N_{nc}} y_{Q,nnc}^2 \right)$$
$$= \sum_{nc}^{2N_{nc}} \left(\frac{y_{nnc}}{\sqrt{N_{nc}}} \right)^2$$ (5)

Because in equation (5) we have the sum of the squares of Gaussian variables, it follows that z has a chi-square distribution, either centrally or non-centrally distributed, depending on whether we have a PP or an OPP. The statistics for these two cases are

$$\begin{cases} z_p \sim \chi^2\left(\hat{E}_b, \dfrac{N_0}{2N_c N_{nc}}, 2N_{nc}\right) \\[2mm] z_o \sim \chi^2\left(0, \dfrac{N_0}{2N_c N_{nc}}, 2N_{nc}\right) \end{cases} \tag{6}$$

where $\chi^2(\psi^2, \sigma^2, d)$ denotes the chi-square distribution with $d = 2N_{nc}$ degrees of freedom, underlying Gaussians of variance

$$\sigma^2 = \frac{N_0}{2N_c N_{nc}},$$

and non-centrality parameter ψ^2. If $\psi^2 = 0$, we have a central chi-square distribution and, if $\psi^2 \neq 0$, we have a non-centrally distributed chi-square. The *cumulative distribution functions* (CDFs) for PP and OPP cases are

$$\begin{cases} F_{\psi^2 \neq 0}(z_p) = 1 - Q_{N_{nc}}^M\left(\sqrt{\dfrac{2N_c N_{nc} E_b}{N_0}}, \sqrt{\dfrac{2N_c N_{nc} z_p}{N_0}}\right) \\[3mm] F_{\psi^2 = 0}(z_o) = 1 - \exp\left\{-\dfrac{z_o N_c N_{nc}}{N_0}\right\} \displaystyle\sum_{k=0}^{N_{nc}-1} \dfrac{1}{k!}\left(\dfrac{z_o N_c N_{nc}}{N_0}\right)^k \end{cases} \tag{7}$$

where Q^M is the generalized Marcum Q function.

Derivation of the Level–Crossing–Rate Estimator

Traditionally, the *level crossing rate* (LCR) information has been widely used in the field of wireless communications for optimizing various receiver parameters, such as modulation format, frame length, and automatic gain control (AGC). LCR information is also used for computing the average error performance of beamforming receivers and estimating the maximum Doppler frequencies or the speed of a mobile receiver.

In the context of satellite-based positioning, usage of LCR information has been rather sparse and only in connection with fading channel characterization and Doppler spread estimation. Despite this, the concept of associating LCR with accurate CNR estimation is, according to our knowledge, completely new.

In earlier work (the paper by D. Skournetou listed in the Additional Resources section near the end of this article), we have demonstrated that the LCR at a certain level of a non-coherently averaged CCF can be indicative of the CNR used to characterize a post-processed signal. For example the LCR has been used as a switch to show whether the signal is below or above a certain CNR level.

Starting from results in the article by D. Skournetou and based on the theoretical model described previously, we developed a method that uses the LCR information in order to produce CNR estimates.

We denote LCR_{down} and LCR_{up} as the number of times a level β is crossed downwards or upwards, respectively. Then, the total number of crossings can be found as
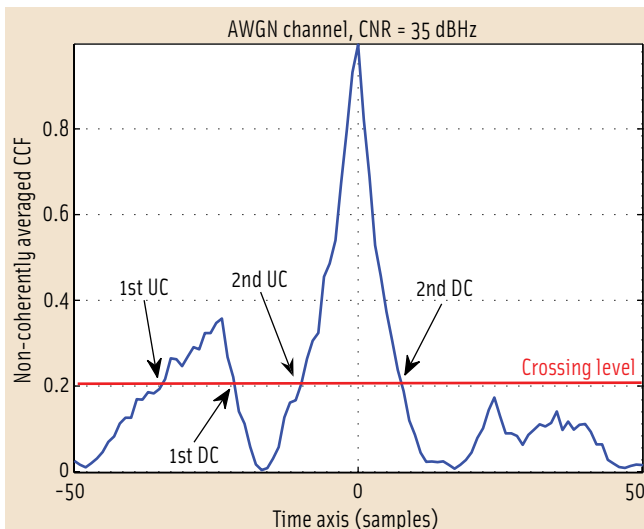
FIGURE 2 **Example of downward and upward crossings, ß = 0.2, N_C = 10 ms, N_{nc} = 2 blocks**

$$LCR_{tot}(\beta) = LCR_{down}(\beta) + LCR_{up}(\beta) \quad \text{(8)} \qquad \text{(8)}$$

In order to define the number of downward and upward crossings, we denote by $z^{(k)}$ as the sample of the non-coherent averaged CCF, and $K_{tot} = N_s N_B W$ as the total number of samples situated within a correlation window of length W chips, and an oversampling factor of N_s, measured as the number of samples per BOC interval. N_B is the BOC modulation order, where, for example, a signal is modulated using a multiplexed BOC (MBOC) scheme, then N_B=12. We may then describe as

$$\begin{cases} LCR_{down}(\beta) = \dfrac{1}{K_{tot}} card\left\{k \middle| \left(z^{(k)} \leq \beta\right) \text{ AND } \left(z^{(k+1)} \geq \beta\right)\right\} \\[2mm] LCR_{up}(\beta) = \dfrac{1}{K_{tot}} card\left\{k \middle| \left(z^{(k)} \geq \beta\right) \text{ AND } \left(z^{(k+1)} \leq \beta\right)\right\} \end{cases} \quad \text{(9)}$$

where "*card*" denotes the cardinality of a set (i.e., the number of elements that belong in this set).

Figure 2 shows examples of upward (UC) and downward (DC) crossings. Note that two upward and two downward crossings occur on level β=0.2 and result in a total of four crossings, such that $LCR_{tot}(0.2) = 4$.

Starting from equation (9), we redefine downward and upward LCRs in terms of probabilities and equivalent CDFs. For example, the probability $z^{(k)}$ to be less or equal to a level β can be found by computing the CDF of the random variable $z^{(k)}$ at β.

Because the random variable corresponds to a sample of the non-coherent CCF, we distinguish among four cases. **Table 1** describes the level crossing rate function for each of these.

In the first case (C1), we have a PP followed by a PP, illustrated in Figure 1 by the blue portion of the curve. The number of such points can be found by counting the number of samples within chip from the maximum peak, τ_{max}, in the CCF, such that we have $2N_s N_B + 1$ points.

The second and third cases are described by (C2) when an OPP is followed by a PP, as illustrated in Figure 1 by the

Case	$z^{(k)}$	$z^{(k+1)}$	$LCR_C^{(k)}$
C1	PP	PP	$LCR_{C1}^{(k)} = F_{\psi^2 \neq 0}^{(k)}(\beta)\left(1 - F_{\psi^2 \neq 0}^{(k+1)}(\beta)\right)$
C2	OPP	PP	$LCR_{C2}^{(k)} = F_{\psi^2 = 0}^{(k)}(\beta)\left(1 - F_{\psi^2 \neq 0}^{(k+1)}(\beta)\right)$
C3	PP	OPP	$LCR_{C3}^{(k)} = F_{\psi^2 \neq 0}^{(k)}(\beta)\left(1 - F_{\psi^2 = 0}^{(k+1)}(\beta)\right)$
C4	OPP	OPP	$LCR_{C4}^{(k)} = F_{\psi^2 = 0}^{(k)}(\beta)\left(1 - F_{\psi^2 = 0}^{(k+1)}(\beta)\right)$

TABLE 1. LCR functions for all point combinations.

both variables are characterized by the same CDF, highlighted by the red curve in Figure 1. The total number of points in this case, is $K_{tot} - 2N_s N_B - 1$.

The number of level crossings over the whole correlation window length can be obtained by adding the partial LCRs given in Table 1 as

$$LCR_{total}^{(\beta)} = \frac{1}{K_{tot}}\left[\sum_{k=\tau_{\max}-N_s N_B}^{\tau_{\max}+N_s N_B} LCR_{C1}^{(k)} + LCR_{C2}^{(k)} + LCR_{C3}^{(k)} + \left(K_{tot} - 2N_s N_B - 1\right)LCR_{C4}^{(k)}\right] \quad \text{(10)}$$

If we assume that the bit energy and channel's amplitude attenuation are known or estimated at the receiver, then $LCR_{total}^{(\beta)}$ depends only on the unknown noise power and the CNR can be computed as

$$CNR\,[\text{dBHz}] = 10\log_{10}\left(\frac{E_b}{N_0}\right) + 10\log_{10}(B_c)$$

$$= \left(\frac{E_b}{N_0}\right)_{dB} + (B_c)_{dBHz} \quad \text{(11)}$$

where B_c is the code epoch bandwidth equal to 1 kHz and $(B_c)_{dBHz} = 30$.

In order to estimate CNR, we compute $LCR_{total}^{(\beta)}$ at level $\beta = median\,(z^{(k)})$, $k = 1, \dots K_{tot}$ for different trial values of CNR. We compute the crossing level at the median because we empirically found that it varies according to the CNR. Although we identify no

CNR Estimators	Estimated CNR [dBHz]
LCRE	$\widehat{CNR} = \arg\max_{CNR}\left(LCR_{total}^{(\beta)}(CNR)\right), \; \beta = median\left(z^{(k)}\right), \; k = 1, \dots K_{tot}$
1stOM	$\widehat{CNR} = 10\log_{10}\left(\frac{E(z_p) - E(z_o)}{E(z_o)N_c}\right) + (B_c)_{dBHz}$
2ndOM	$\widehat{CNR} = 10\log_{10}\left(-\frac{1+N_{nc}}{N_c N_{nc}} + \frac{1}{N_c}\sqrt{\left(1 + \frac{1}{N_{nc}}\right)\left(\frac{E(z_p^2)}{E(z_o^2)} + \frac{1}{N_{nc}}\right)}\right) + (B_c)_{dBHz}$
NWPR	$\widehat{CNR} = 10\log_{10}\left(\frac{1}{N_{nc}}\sum_{nnc=1}^{N_{nc}}\left(\frac{1}{T}\frac{NP_{ncc}-1}{N_c - NP_{ncc}}\right)\right), \; T = 1\text{ ms}$ $NP_{nnc} = \frac{WBP_{nnc}}{NBP_{nnc}}$ $WBP_{nnc} = \sum_{i=1}^{N_c}\left(x_{I,i}^2 + x_{Q,i}^2\right)$ $NBP_{ncc} = \left(\sum_{i=1}^{N_c} x_{I,i}\right)^2 + \left(\sum_{i=1}^{N_c} x_{Q,i}\right)^2$

TABLE 2. List of CNR estimators.

left edge of the blue curve, and (C3) PP is followed by an OPP, as illustrated by the right edge of the blue curve.

Finally, in the fourth case (C4), where an OPP is followed by an OPP,

formulation of the exact dependency, we do not need it for the derivation of estimator.

To calculate the partial LCRs defined in Table 1, we use the CDF output for each chosen level.

Look-Up Table Reduces Computing Time

In order to reduce the complexity of the algorithm, we compute the CDFs for different level crossings and store the values in a look-up table. After the median of the CCF is computed, we compare it with those in the look-up table and choose the CDF output with the best level crossing match.

After calculating the total number of crossings using equation (10), we estimate CNR as

$$\widehat{CNR} = \arg\max_{CNR}\left(LCR_{total}^{(\beta)}(CNR)\right) \quad \text{(12)}$$

In other words, the estimated CNR is indicated by the trial CNR value resulting in the maximum number of level crossings. **Figure 3** shows an example the $LCR_{total}^{(\beta)}$ function computed for a single-path AWGN channel with a CNR equal to 40 dBHz.

We recall that LCRE is based on the assumption that the bit energy (E_b) and the signal's amplitude attenuation (a_0) are known at the receiver side. When this is not the case, a two-dimensional search of the look-up table should be performed, computing the total number of level crossings first, for different values of the product $E_b a_0^2$, and then for the different CNRs.

CNR Estimators

Typical CNR estimators for GNSS signals are based on the first- or higher order moments of the CCF output. Among the least computationally demanding, we find the first- and second-order moment (1stOM and 2ndOM, respectively) based estimators with which to estimate CNR, using the equations shown in **Table 2**. Starting from the earlier theoretical derivations, we define the mean and variance of OPPs and PPs, respectively, as
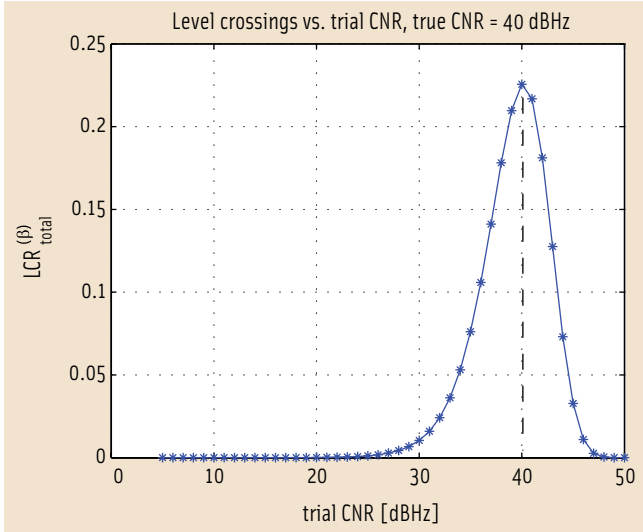
FIGURE 3 Total number of level crossings versus trial CNR values in single–path AWGN channel, true CNR = 40 dBHz (ß =0.008).

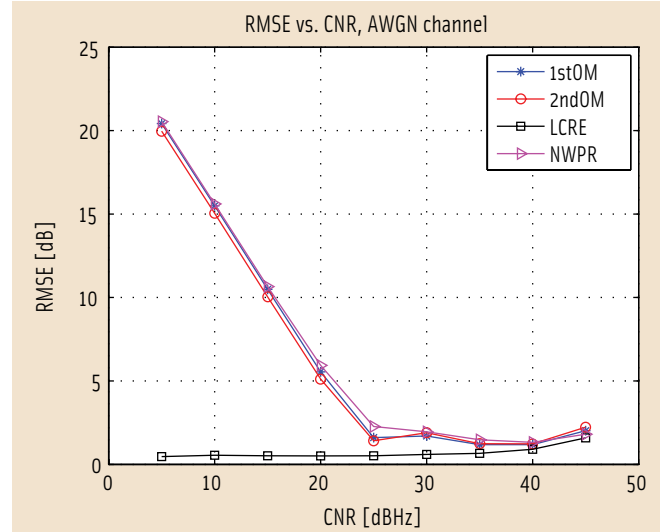FIGURE 4 RMSE of CNR estimation vs. true CNR in single–path AWGN channel.

$$\begin{cases} E\left(z_o\right) = \dfrac{N_0}{N_c} \\ E\left(z_o^2\right) = \dfrac{N_0^2}{N_c^2}\left(\dfrac{1}{N_{nc}} + 1\right) \end{cases} \quad (13)$$

$$\begin{cases} E\left(z_p\right) = \dfrac{N_0}{N_c} + \hat{E}_b \\ E\left(z_p^2\right) = \dfrac{N_0}{N_c}\left(\dfrac{1}{N_{nc}} + 1\right)\left(2\hat{E}_b + \dfrac{1}{N_c}\right) + \hat{E}_b^2 \end{cases} \quad (14)$$

For ergodic processes, the statistic average is equal to the time average. However, since we usually have only one observation of the correlation function, we typically have only one, or very few, PPs and several OPPs. Thus, we have

$$\begin{cases} E\left(z_p^i\right) \approx z_p,\ i = 1, 2 \\ E\left(z_o^i\right) \approx \dfrac{1}{K_{OPP}} \displaystyle\sum_{k=1}^{K_{OPP}} z_{o,k}^i,\ i = 1, 2 \end{cases} \quad (15)$$

where $K_{OPP} \geq 1$ is the number of OPPs used to estimate the mean.

Another popular CNR estimator is based on the ratio of the signal's wide-band power (WBP) to its narrowband power (NBP), known as the *narrow-band-wideband-power-ratio* (NWPR) estimator. The formulas with which NWPR method estimates CNR can also be found in Table 2.

For a fair comparison of the CNR estimators, we do not use any smoothing factor in the NWPR method, because the rest of the methods produce a CNR estimate using a single instance of CCF. This means that only one value of *NP* is available for computation of the CNR; however, in practice actual receivers may use an average of *NP* over few hundreds of instances in order to produce one estimate.

Comparing Estimators' Performance

In this section, we compare the simulation results based on performance of the four CNR estimators: 1stOM, 2ndOM, the proposed LCRE, and NWPR. In order to create a fair comparison, we use the same number of OPPs in the moment-based estimators as in our LCRE method, described by $K_{OPP} = K_{tot} - 2N_s N_B - 1$.

The simulations were carried out assuming an infinite bandwidth, a rectangular pulse shaping filter, and an oversampling factor of $N_s = 4$, where each BOC interval contained four samples. The BOC order was $N_B = 12$, and we set the time-bin equal to $1/(N_s N_B)$ millisecond, which is the interval between samples of the correlation function. The smaller the interval is, the more bins along the correlation function we have. Moreover, the output of the correlation function is coherently averaged using $N_c = 10$ milliseconds, followed by two blocks of non-coherent integration ($N_{nc} = 2$).

Unless we have single-path channel, the number of paths is uniformly distributed between L_{min} and L_{max}. We assume the path separation between successive paths at any time instance to be uniformly distributed between 0 and 0.35 chips, simulating closely-spaced paths, typically found in indoor and densely populated urban scenarios.

Finally, under the condition of fading channels we used Nakagami-m type, where the Nakagami m-factor was equal to 0.8.

In cases where we deviate from these values or needed additional parameters to describe the simulation setup, we note this in the title and/or caption of the figures. As the performance metric we use the root mean square error (RMSE) between the true and the estimated CNR, computed over 500 random channel realizations.

Figure 4 illustrates the RMSE values versus the true CNR when the channel is AWGN. LCRE performs significantly better in the region of very low CNRs, below 25 dBHz, while NWPR and the moment-based estimators achieve small estimation errors when the true CNR is 25 dBHz or higher.

In this scenario the NWPR method performs the best for CNR greater than 50 dBHz. Because our emphasis is on
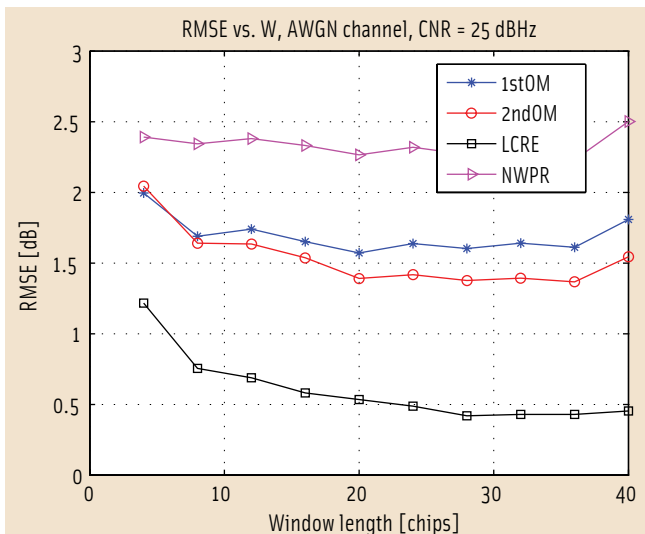
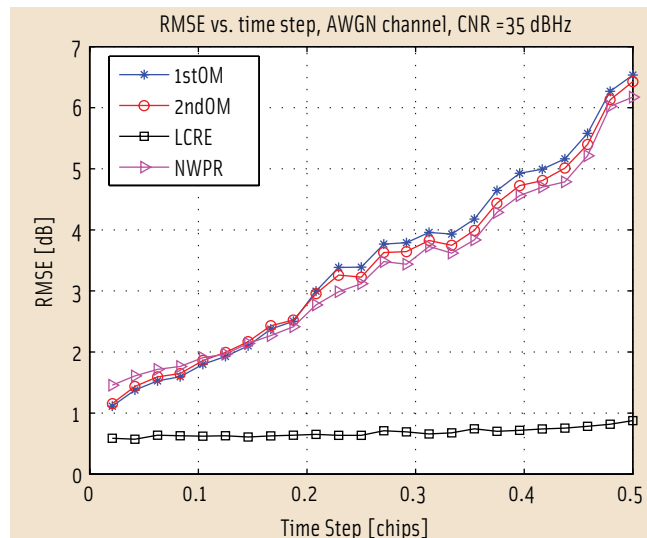FIGURE 5 RMSE vs. correlation window length (W) in single-path AWGN and CNR = 25 dBHz.

FIGURE 6 RMSE versus time step in single-path AWGN channel and CNR = 20 dBHz.

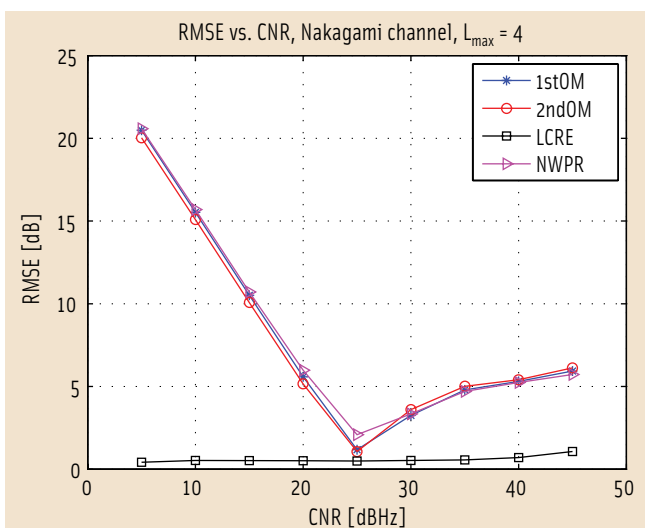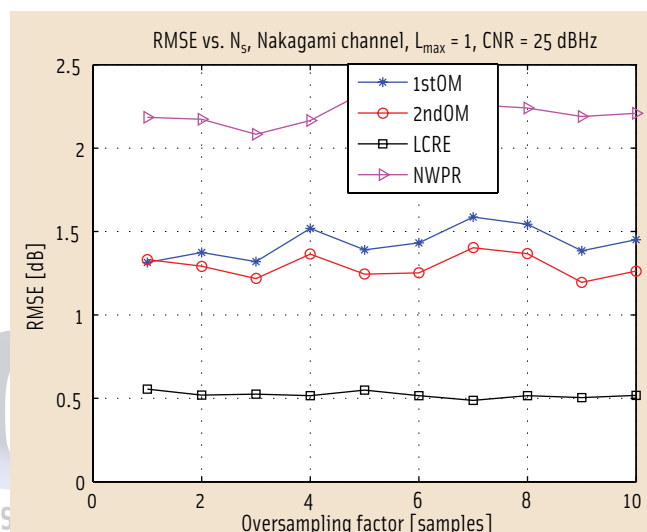FIGURE 7 RMSE of CNR estimation vs. true CNR in Nakagami channel.

FIGURE 8 RMSE versus oversampling factor (Ns) in Nakagami channel and CNR = 25 dBHz.

low to high CNR levels, the result for the very high CNR range, up to 65 dBHz, was not included.

Figure 5 shows the performance of the estimators for different correlation window lengths in AWGN channel, and when the true CNR is 25 dBHz. In this case the performance of LCRE improves as the correlation window length increases; however, the window length does not significantly affect any of the four estimators.

Figure 6 shows how the size of scanning the correlation function in the time domain affects the estimators where CNR = 35 dBHz. At this CNR level, the performance of moment-based estimators and NWPR deteriorates with decreasing temporal resolution, while LCRE maintains an almost constant performance.

In **Figure 7**, we see the performance of the estimators in the fading channel when the maximum number of paths is four. Here, the performance of LCRE is also almost constant over the CNR range, while the rest of the estimators are affected by the presence of multipath, even under good CNR conditions. **Figure 8** depicts RMSE versus the oversampling factor in the single-path fading channel, with CNR equal to 20 dBHz.

At this low CNR value, no significant effects are observed.

Figures 9 and **10** illustrate the effect of the maximum number of channel paths in Nakagami-m channel for CNR equal to 20 and 35 dBHz, respectively. As expected, for very low CNRs the effect of channel paths is less evident than for higher CNRs, when signal can be distinguished from channel noise. Again, the LCRE performs consistently, regardless of the maximum number of paths, for CNR = 35 dBHz. The performance of the other three estimators deteriorates with increasing paths.

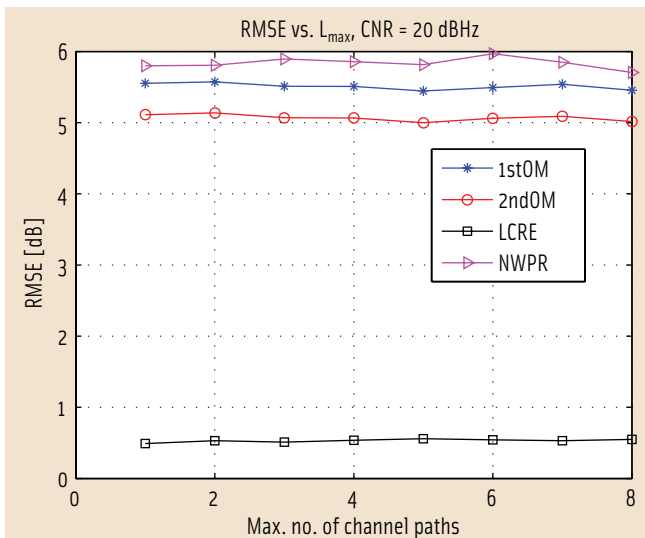The effects of finite bandwidth (B_w)

FIGURE 9 RMSE versus maximum number of channel paths in Nakagami channel and CNR = 20 dBHz.
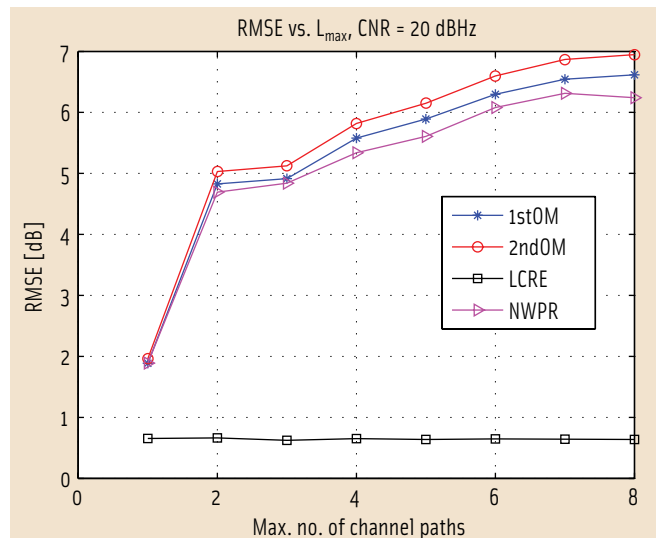

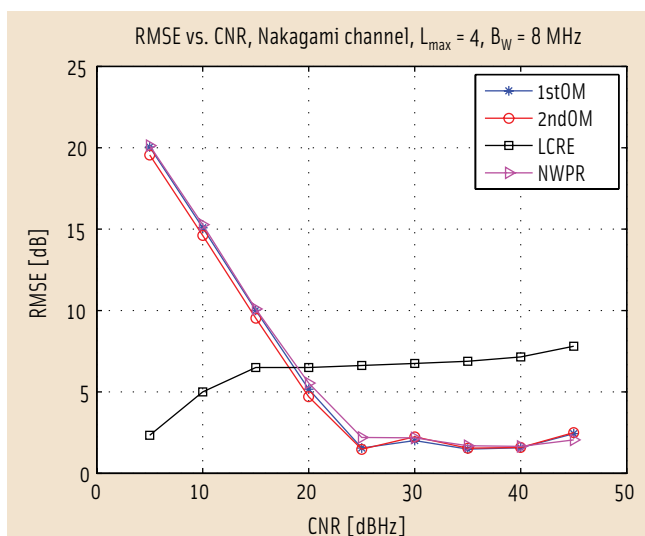FIGURE 10 RMSE versus maximum number of channel paths in Nakagami channel and CNR = 35 dBHz.

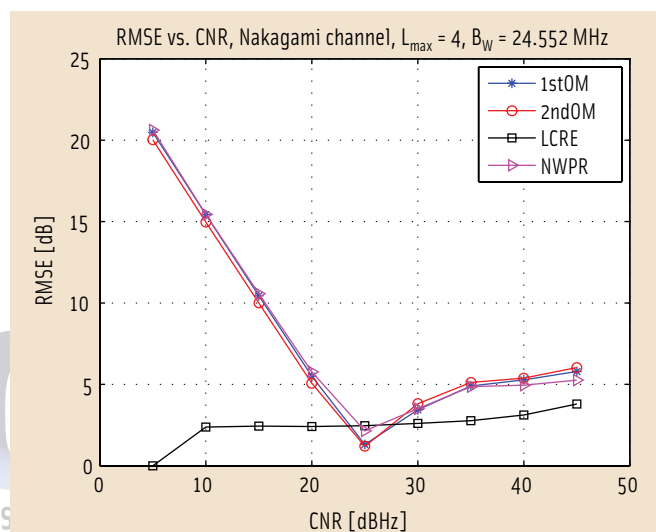FIGURE 11 RMSE of CNR estimation vs. true CNR in Nakagami channel and BW = 8 MHz.

FIGURE 12 RMSE of CNR estimation versus true CNR in Nakagami channel and BW = 24.552 MHz.

are depicted in Figures 11 and 12. In the first case, we used B_W = 8 MHz and a Butterworth filter with 0.1 decibel loss in pass-band, 40-decibel attenuation in stop-band, and a transition bandwidth equal to BW/2. Comparison of **Figure 11** with Figure 7 indicates that only the LCRE method was negatively affected by the limited bandwidth case, while the rest of the methods remained unaffected.

Nonetheless, LCRE performs best only in the very low CNR region, below 20 dBHz, while for regions from low to high CNR values, moment-based and NWPR methods perform the best. In the

second case illustrated in **Figure 12**, we used receiver bandwidth BW = 24.552 MHz, which is the same as that used for the transmission of Galileo E1 signal. In this case, LCRE clearly performs better than other methods, except where CNR = 25 dBHz. Moreover, we notice that unlike the LCRE method, the moment-based and NWPR methods perform better at 8 MHz bandwidth than at 24.552 MHz for CNR greater than 25 dBHz.

Summary and Conclusions

We introduce and derive a new method for estimating CNR, called Level Cross-ing Rate-based-Estimator (LCRE), by exploiting statistical characteristics of correlation samples. We compare the LCRE method with first- and second-based moments, as well as with the well-known Narrowband-Wideband Power Ratio method.

The performance comparison covers both cases of Additive White Gaussian Noise (AWGN) and fading multipath channels. The former is used for investigating the maximum achievable performance, while the latter is chosen for the representation of more realistic scenarios.

Results show the proposed LCRE method performs considerably better than the other three methods under very low CNR conditions, ranging from 5 to 20 dBHz or higher, depending on the scenario. However, the improved performance of LCRE is counterbalanced by its higher computational complexity, mitigated by the implementation of a look-up table.

In cases where low computational complexity is required, the NWPR method provides the best solution. Although the algorithm designer must decide how much computational complexity to trade for improved accuracy, the use of look-up tables reduces the LCRE execution speed.

Acknowledgements

Additional Resources

[1] Falletti, E.. and Pini, M. and Lo Presti, L. "Are C/N_0 algorithms equivalent in all situations?" Inside GNSS, vol. 5, No. 1, January/February, 2010

[2] Islam, A.K.M.N., and E. S. Lohan, and M. Renfors, "Moment-based CNR estimators for BOC/BPSK modulated signal for Galileo/BPSK," WPNC, Hannover, Germany, March 2008

[3] Lohan, E. S., "Statistical analysis of BPSK-like techniques for the acquisition of Galileo Signals," in Proceedings of 23rd AIAA International Communications Satellite Systems Conference (IC-SSC), September 2005

[4] Lohan, E. S., "Analysis of Filter-Bank-Based Methods for Fast Serial Acquisition of BOC-Modulated Signals," EURASIP Journal on Wireless Communications and Networking, Volume 2007, Article ID 25178, 12 pages, doi:10.1155/2007/25178.

[5] Proakis, J., "Digital Communications", McGraw-Hill, New York, USA, 1995.

[6] Sayre, M. "A Block Processing Carrier to Noise Ration Estimator for the Global Positioning System", in proceedings of ION NTM, 2004, pp. 862-868.

[7] Skournetou, D., and E. S. Lohan, "Indoor location awareness based on the non-coherent correlation function for gnss signals," In Proc. of Finnish Signal Processing Symposium (FINSIG'07), Oulu, Finland, August 2007. Available online at <http://www.cs.tut.fi/tlt/pos/publicat.html>

[8] Tsui, J. B.-Y., Fundamentals of Global Positioning System Receivers: a Software Approach, Wiley Interscience, 2005

[9] Van Dierendonck, A.J. , GPS Receivers" Global Positioning System: Theory and Applications. Vol. 1. Eds. B. W. Parkinson and J. J. Spilker, Jr. Washington, DC: American Institute of Aeronautics and Astronautics, pp. 329-407, 1996

Authors

Elena Simona Lohan is an adjunct professor in the Department of Communications Engineering, Tampere University of Technology, since 2007. She obtained her Ph.D. degree in wireless communications from Tampere University of Technology. She also graduated with an M.Sc. in electrical engineering from "Politehnica" University of Bucharest, Romania, and with a D.E.A. (French equivalent of master's degree) in econometrics from Ecole Polytechnique, Paris, France. She is currently leading the research activities in signal processing for wireless communications in the Department of Communications Engineering, TUT (http://www.cs.tut.fi/tlt/pos/). She is the principal investigator in a research project funded by the Academy of Finland focusing on indoor location and has been involved as technical group leader in two European GNSS-related projects, within FP6 and FP7: "GREAT" and "GRAMMAR," dealing with Galileo mass-market receivers. She has about 80 international journals and conferences articles related to CDMA-based signal processing in navigation and communications.

Danai Skournetou received a B.Sc. degree in informatics and telecommunication from Athens National and Kapodistrian University, Greece, and the M.Sc. degree in information technology from Tampere University of Technology in 2007. Currently, she is a Ph.D. candidate in the Department of Communications Engineering in Tampere University of Technology, Finland. In addition, she is pursuing an M.Sc. degree in economics and business administration from Jyväskylä University, Finland. Her research interests include methods for code and carrier tracking of Galileo and GPS signals, indoor positioning, range estimation, CNR estimation, location-based services (LBS) and technology management. **IG**